Research Article

Comparative enantioseparation of planar chiral ferrocenes on polysaccharide-based chiral stationary phases

Alessandro Dessì,[1,‡] Barbara Sechi,[1,‡] Roberto Dallocchio,[1] Bezhan Chankvetadze,[2] Mireia Pérez-Baeza,[3] Sergio Cossu,[4] Victor Mamane,[5,*] Patrick Pale,[5] and Paola Peluso[1,*]

[1] Istituto di Chimica Biomolecolare ICB, CNR, Sede secondaria di Sassari, Traversa La Crucca 3, Regione Baldinca, I-07100 Li Punti - Sassari, Italy

[2] Institute of Physical and Analytical Chemistry, School of Exact and Natural Sciences, Tbilisi State University, Chavchavadze Ave 3, 0179 Tbilisi, Georgia

[3] Departamento de Química Analítica, Universitat de València, Burjassot, València, Spain

[4] Dipartimento di Scienze Molecolari e Nanosistemi DSMN, Università Ca' Foscari Venezia, Via Torino 155, I-30172 Mestre Venezia, Italy

[5] Institut de Chimie de Strasbourg, UMR CNRS 7177, Equipe LASYROC, 1 rue Blaise Pascal, 67008 Strasbourg Cedex, France

SHORTENED TITLE: ENANTIOSEPARATIONS OF SUBSTITUTED FERROCENES

KEY WORDS: Electrostatic potential / Enantioseparation / Ferrocenes / Planar chirality / Polysaccharide-based chiral stationary phases

CORRESPONDENCE TO:

Dr. Paola Peluso
Istituto di Chimica Biomolecolare ICB CNR – UOS di Sassari,
Traversa La Crucca, 3, Regione Baldinca, I-07100 Li Punti - Sassari, Italy
E-mail address: paola.peluso@cnr.it

Dr. Victor Mamane
Institut de Chimie de Strasbourg, UMR CNRS 7177, Equipe LASYROC,
1 rue Blaise Pascal, 67008 Strasbourg Cedex, France
E-mail address: vmamane@unistra.fr

[‡] These authors contributed equally to this work

Graphical abstract - High-performance liquid chromatography (HPLC) enantioseparations of ten 1,2- and 1,3-disubstituted planar chiral ferrocenes on five polysaccharide-based chiral stationary phases (CSPs) were comparatively explored under multimodal elution conditions. The presence of π-extended systems in the analyte structure was shown to impact affinity of the most retained enantiomer toward amylose-based selectors, observing retention times higher than 80 min with methanol-containing mobile phases (MPs).

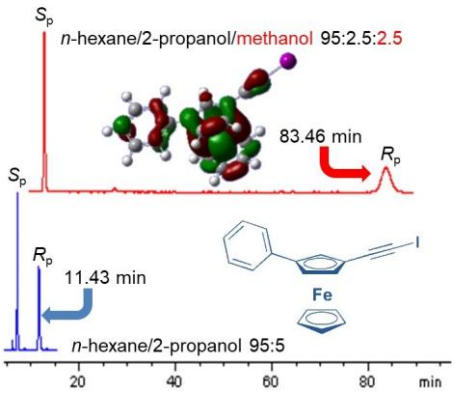

ABSTRACT - Planar chiral ferrocenes are well-known compounds which have attracted interest for application in synthesis, catalysis, material science, and medicinal chemistry for several decades. In spite of the fact that asymmetric synthesis procedures for obtaining enantiomerically enriched ferrocenes are available, sometimes the accessible enantiomeric excess of the chiral products is unsatisfactory. In such cases and for resolution of racemic chiral ferrocenes, enantioselective high-performance liquid chromatography (HPLC) on polysaccharide-based chiral stationary phases (CSPs) has been used in few literature reports. However, while moderate/high enantioselectivities have been obtained for planar chiral ferrocenes bearing polar substituents, the enantioseparation of derivatives containing halogens or exclusively alkyl groups remains rather challenging. In this study, the enantioseparation of ten planar chiral 1,2- and 1,3-disubstituted ferrocenes was explored by using five polysaccharide-based CSPs under multimodal elution conditions. Baseline enantioseparations were achieved for nine analytes with separation factors (α) ranging from 1.20 to 2.92. The presence of π-extended systems in the analyte structure was shown to impact affinity of the most retained enantiomer toward amylose-based selectors, observing retention times higher than 80 min with methanol-containing mobile phases (MPs). Electrostatic potential (*V*) analysis and molecular dynamics (MD) simulations were used in order to inspect interaction modes at the molecular level.

1. INTRODUCTION

Ferrocene ([Fe(η^5-C_5H_5)$_2$]) is an iconic framework in organometallic chemistry,[1] which, in 1952, was characterized as the first sandwich compound by Woodward and co-authors.[2] Structurally, ferrocene is a rigid three-dimensional unit wherein iron is located between two cyclopentadienyl (Cp) rings. Owing to its stability, and the possibility of functionalization at the cyclopentadienyl rings,[3-7] ferrocene derivatives have over time found application in several fields such as catalysis,[8-10] medicinal chemistry,[11] and material chemistry.[12-14] Moreover, the ferrocenium/ferrocene system (Fc/Fc^+) is a versatile redox couple which have proven to be suitable for the preparation of switchable functional systems.[1,15,16]

Due to their versatility to access molecular wires, and responsive switchable systems and materials,[17-19] particular attention has been devoted to the so-called "π-extended ferrocenyl frameworks", which are featured by delocalized orbital networks based on the combination of a ferrocene unit and a π-conjugated extended cloud, such as the ethynyl group.[13,20] Planar chiral aryl ethynyl ferrocenes have been used as intermediates for the preparation of helical ferrocenes showing peculiar chiroptical properties with very high optical value and huge intensity of the CD signals.[21]

Recently, our groups developed the design, synthesis, and characterization of compounds **1**-**8** as new chiral iodoethynyl ferrocenes showing three key features (Figure 1):[6] *a)* planar chirality due to the presence of two different substituents on the same Cp ring, *b)* a π-extended ethynyl ferrocenyl moiety, with the possibility to further extend the π-conjugation to the second Cp-substituent depending on its electronic features (Figure 2a,b), and *c)* an iodine substituent as an electrophilic σ-hole donor activated by C≡C group (Figure 2d).[22,23] In this regard, it is worth mentioning that halogen bonds (XBs) were identified in the crystal packing of compounds **1**, **3**-**5**, and **7** with both lengths and angles falling within the range of values typically observed for this type of σ-hole bonds.[6]

These features also make compounds **1**-**8** suitable as test probes to explore the impact of both π-extended clouds and electrophilic σ-holes in enantioselective processes occurring in HPLC environment, with the aim to profile noncovalent interactions involved in the enantioselective recognition. In previous

studies, we demonstrated that σ-hole interactions, such as XBs and chalcogen bonds (ChBs), which involve electrophilic regions of electron charge density depletion (σ-holes), may participate in the enantioselective interaction between polysaccharide-based selectors and selectands containing electrophilic σ-holes.[24-27]

On this basis, we explored the enantioseparation of chiral ferrocenes **1**-**8** along with **9** and **10**, as reference compounds for comparison, by using five polysaccharide carbamate-based chiral stationary phases (CSPs) (Supporting Information, Table S1) under multimodal elution conditions. The experiments were integrated with computational analysis by using electrostatic potential (*V*) calculations and molecular dynamics (MD) simulations in order to disclose the mechanistic features of these enantioseparations.

The second aim of this study was to identify suitable methods for baseline enantioseparation of chiral ferrocenes containing small or nonpolar groups. Indeed, while moderate/high enantioselectivities have been obtained under normal-phase (NP) elution conditions for planar chiral ferrocenes bearing hydroxyl, carbonyl, and carboxyl groups as substituents,[21,28-30] the enantioseparations reported for derivatives containing small groups, halogens or exclusively alkyl groups are rather unsatisfying.[31,32] It is worth mentioning that few papers have reported systematic studies on enantioseparation of organometallic compounds on polysaccharide-based CSPs so far.[28,31-39]

2. MATERIALS AND METHODS

2.1. Chemicals and reagents

Compounds **1**-**10** were prepared and characterized as previously reported.[6,40] HPLC grade *n*-hexane (Hex), methanol (MeOH), isopropyl alcohol (IPA), acetonitrile (ACN) and water were purchased from Sigma-Aldrich (Taufkirchen, Germany).

2.2. Chromatography

An Agilent Technologies (Waldbronn, Germany) 1100 Series HPLC system (high-pressure binary gradient system equipped with a diode-array detector operating at multiple wavelengths (220, 254, 280,

360 nm), a programmable autosampler with a 20 μl loop, and a thermostated column compartment) was employed. Data acquisition and analyses were carried out with Agilent Technologies ChemStation Version B.04.03 chromatographic data software. The UV absorbance is reported as milliabsorbance units (mAU). Lux Cellulose-1 (C-1) (cellulose *tris*(3,5-dimethylphenylcarbamate), CDMPC), Lux i-Cellulose-5 (iC-5) (cellulose *tris*(3,5-dichlorophenylcarbamate), CDCPC), Lux Amylose-1 (A-1) and Lux i-Amylose-1 (iA-1) (amylose *tris*(3,5-dimethylphenylcarbamate), ADMPC), and Lux i-Amylose-3 (iA-3) (amylose *tris*(3-chloro-5-methylphenylcarbamate), ACMPC) (5 μm) (Phenomenex Inc., Torrance, CA, USA) were used as chiral columns (250 × 4.6 mm) (Table S1). Analyses were performed in isocratic mode at 25°C. The flow rate (*FR*) was set at 0.8 ml/min. For compounds **1**, **3**-**6**, **7**, and **8**, the enantiomer elution order (EEO) was determined by injecting enantiomers of known absolute configuration prepared by asymmetric syntheses.[6] For compounds **9** and **10**, the relative EEO was assigned by injecting pure enantiomers of unknown absolute configuration which are denoted as X_9, Y_9 and X_{10}, Y_{10}.

2.3. Computationals

V extrema calculated on the molecular electron density isosurfaces (maxima and minima) ($V_{S,max}$ and $V_{S,min}$) (au, electrons/bohr) were computed by using Gaussian 09 (Wallingford, CT 06492, USA),[41] at the density functional theory (DFT) level of theory, using the B3LYP functional and the def2TZVPP basis set. Search for the exact location of $V_{S,max}$ and $V_{S,min}$ was made through the Multiwfn code[42] and through its module enabling quantitative analyses of molecular surfaces (isovalue 0.002 au).[43] In our computations, .wfn files were obtained through the Gaussian 09 package. Details for molecular dynamics (MD) are reported in the Supporting Information file.

3. RESULTS AND DISCUSSION

3.1. Chromatographic screening

In the frame of this study, analytes, CSP and mobile phase (MP) were considered as experimental variables, examined individually, and their influence on retention and selectivity was examined through

the evaluation of retention and separation factors (*k* and α), on the basis of the following preliminary remarks:

a) within the 1,2-disubstituted **1**-**5** and 1,3-disubstituted **6**-**8** series, the influence of the distinctive functional group on enantioseparation was evaluated. As shown in Figure 2, different substituents on the Cp ring may determine different degrees of delocalization across the entire system. For instance, for compound **4** (Ph) and **5** (2-Naphth) (Figure 2b,c) the delocalization is across the entire molecule, whereas for compound **3**, the calculated HOMO does not extend on the second substituent (Me) (Figure 2a). The impact of the triple bond on the enantioseparation was examined, and for this purpose compounds **9** and **10** served as reference systems for comparison. The effect of 1,2- and 1,3-disubstitution on the enantioseparation was also considered. The local electron charge density of specific molecular regions of the analytes was inspected in terms of calculated V_S (Supporting Information, Table S2), positive and negative V_S values being associated with electrophilic and nucleophilic regions;

b) the performances of different polysaccharide selectors were evaluated under multimodal elution conditions, and compared in terms of polysaccharide backbone (cellulose-based C-1 *versus* amylose-based A-1), and type of carbamate pendant groups (methylated A-1, iA-1, C-1, chlorinated iC-5, methylated and chlorinated iA-3). In this regard, the electronic properties of the carbamate moiety, which are tuned by methyl and chlorine substituents located on the phenyl ring of the carbamate pendant groups, were determined by DFT calculations (Table 1). The impact of the anchoring technique (immobilization *versus* coating)[44,45] was also considered by comparing the performances of amylose *tris*(3,5-dimethylphenylcarbamate) (ADMPC)-based columns (A-1 *versus* iA-1);

c) the effect of MP on the enantioseparations was evaluated comparatively by using *n*-hexanic mixtures (Hex/IPA 95:5 (A) and Hex/IPA/MeOH 95:2.5:2.5 (B) v/v), polar organic (PO) conditions (MeOH 100% (C)), and aqueous-organic mixtures (MeOH/water 95:5 (D) and 90:10 € v/v). In particular, the comparative use of A-E, as MPs, allowed for evaluating the effect of increasing hydrophobicity of the medium. The introduction in the MP of 2.5% MeOH (B) allows modulation of the

binding between analyte and polysaccharide-based selector by favouring a better penetration of the analyte into the groove, and tuning hydrophobic *versus* hydrogen bond (HB) interactions,[46,47] while keeping intact the high-ordered three-dimensional structure of the polysaccharide. Otherwise, the use of pure MeOH (C), as a MP, impacts intramolecular HBs determining the high-ordered structure of the polysaccharide, thus producing a huge effect within the polysaccharide structure.[46-49] In particular, the hydroxyl groups of MeOH molecules strongly interact, as HB donors/acceptors, with C=O and N-H groups of the polymer, competing with intramolecular HBs within the selector, and with selector-selectand intermolecular HBs.[46,50] Indeed, with MeOH, hydrophobic interactions tend to be more favoured compared to HBs, and the addition of water was expected to enhance hydrophobic interactions and increase capacity factors in accordance with a typical reversed-phase (RP) system.[51]

On this basis, twenty-five chromatographic systems generated by the combination of C-1, iC-5, A-1, iA-1, and iA-3 with the mixtures A-E, as MPs, were evaluated and characterized by *k* (Supporting Information, Figure S1) and α (Figure S2) values toward ferrocenes **1**-**10** (Tables S3-S12). Baseline enantioseparations were obtained for compounds **1**-**8** and **10** with α values ranging from 1.10 to 11.41, whereas partial enantioseparation (α = 1.07) was obtained only for **9**, with the system C-1/A. For compounds **1**, **3**, and **10**, baseline enantioseparations were achieved under NP elution conditions and with aqueous-MeOH mixtures as MPs, but MeOH showed to exert a detrimental effect on the enantioseparation in these cases. Compounds **2**, and **4**-**8** were baseline enantioseparated under all three elution modes, namely *n*-hexanic mixtures, PO and aqueous-organic elution conditions. Chromatographic conditions and parameters of the best enantioseparations obtained for compounds **1**-**8** and **10**, as a suitable compromise between a sufficiently high enantioselectivity value, a baseline resolution, and a run time as short as possible, are reported in Table 2 (see Supporting Information, Figure S3 for chromatographic traces). For compounds **3**-**5**, **7**, and **8** optimized enantioseparations were obtained by using chlorinated chiral columns (iA-3 or iC-5) with selectivity factors ranging from 1.46 to 2.92. Otherwise, for compounds **1**, **2**, **6**, and **10**, optimized enantioseparation methods were developed

by using coated methylated chiral columns (C-1 or A-1) ($1.19 \leq \alpha \leq 2.13$). In the series of optimized enantioseparations, methanol-containing MPs were successfully used for compounds **1**-**4**, **6**, and **10**, and NP elution conditions for **5**, **7**, and **8**.

3.2. Impact of analyte structure on enantioseparation

With the aim to evaluate the impact of the structural features of each analyte on its enantioseparability, the rate of baseline enantioseparations (*rbs*) was determined from the wealth of chromatographic results (Figure 3). In the frame of the twenty-five chromatographic systems explored in this study, *rbs* increased following the order **7**, **8** (64%, 62%) > **2** (32%) > **4**,**5** (28%) > **6** (16%) > **3**,**10** (12%) > **1** (8%) > **9** (0%). From this trend, some remarks emerged:

a) 1,3-disubstituted ferrocenes showed high enantioseparability compared to the 1,2-disubstituted analogues (**7** > **4**, **8** > **5** and **6** > **1**). Indeed, average retention factors (Figure S4a) and selectivity factors (Figure S4b) of **6**, **7**, and **8** ($1.56 \leq k \leq 11.88$; $1.05 \leq \alpha \leq 3.45$) were, in general, higher than those of **1**, **4**, and **5** ($0.65 \leq k \leq 1.62$; $1.05 \leq \alpha \leq 1.32$), respectively. This behaviour could be caused by the fact that in the 1,3-pattern both substituents are accessible to the selector, whereas the substituents are sterically constrained in 1,2-substituted derivatives. On the other hand, no relevant difference in terms of V_S values (Table S2), justifying the different *rbs*, was observed between 1,2- and 1,3-substituted derivatives;

b) the ethynyl framework represents a key structural element given that the enantioseparability decreased moving from **1** and **2** (*rbs*: 8% and 32%) to **9** and **10** (*rbs*: 0% and 12%), respectively. In terms of V_S values associated to nucleophilic and electrophilic region, it is worth mentioning that in **1** and **2** the ethynyl group contributes to increase the electrophilic character of the iodine ($V_{S,max}$ (I) = 0.0721 au (**1**) and 0.0755 au (**2**)), compared to the analogues **9** and **10** ($V_{S,max}$ (I) = 0.0465 au (**9**) and 0.0529 au (**10**)), respectively. Interestingly, both *rbs* and positive $V_{S,max}$ on iodine decreases along the bromoiodo-substituted series **6** (*rbs* 16%, $V_{S,max}$ (I) = 0.0737 au), **1** (*rbs* 8%, $V_{S,max}$ (I) = 0.0721 au), **9** (*rbs* 0%, $V_{S,max}$ (I) = 0.0465 au). In addition, compound **2** presents higher electron density on the C≡N

group ($V_{S,min}$ (N) = -0.0721 au) and a more extended π-system compared to the analogue **10** ($V_{S,min}$ (N) = -0.0714 au);

c) the presence of a π-extended system involving the second substituent of the iodoethynyl ferrocene impacts both retention and selectivity. Indeed, compounds **2**, **4**, **5**, **7**, and **8** showed average retention for both first and second eluted enantiomer, average selectivity and *rbs* ($0.76 \leq k \leq 11.88$; $1.20 \leq \alpha \leq 3.45$; $28\% \leq rbs \leq 64\%$) higher compared to compounds **1**, **3**, **6**, **9**, and **10** ($0.54 \leq k \leq 1.64$; $1.01 \leq \alpha \leq 1.11$; $0\% \leq rbs \leq 16\%$);

d) the EEO was determined for each enantioseparation, and the assignments are summarized in Table S5 (Supporting Information). *S*-*R* was the most frequent EEO, and only compound **2** retained its EEO in all chromatographic systems. Several cases of reversal of EEO dependent on analyte structure, selector structure, and MP type could be observed, but in general they are not easy to explain. Compounds containingπ-extended systems provided interesting cases of EEO. For instance, on C-1/A and C-1/B all compounds showed *S*-*R* as EEO with the exception of **7** and **8** (*R*-*S*). Interestingly, by changing the *n*-hexanic mixtures to pure MeOH with the same chiral column (C-1/C), only compound **8** retained the *R*-*S* sequence as EEO, whereas compound **7** showed MP-dependent EEO reversal to *S*-*R*, despite the structural similarity of the two analytes. Compound **5** showed the *S*-*R* elution order on all amylose-based selectors with mixture A, but adding 2.5% MeOH provided EEO reversal to *R*-*S* on the same selectors. Again, only for compound **5**, a reversal of elution order was observed on immobilized iA-1 (*R*-*S*) compared to the coated A-1 (*S*-*R*) by using MeOH or the aqueous mixture D as MPs. The same phenomenon was not observed with *n*-hexanic mixtures (mixtures A and B).

3.3 Impact of selector structure on enantioseparation

Among the chiral columns used in this study, better results were obtained on the A-1 and iA-3, each column providing baseline enantioseparations for seven compounds. C-1 was also able to enantioseparate six compounds, whereas iC-5 and iA-1 provided baseline enantioseparations only for compounds **2**, **4**, **5**, **10** and **7**, **8**, respectively (Supporting Information, Figure S6). Compounds **2** and **10**

containing the C≡N group as a strong HB acceptor showed very high retention on the iC-5 ($5.39 \leq k \leq 6.29$) under NP conditions, but moderate selectivity on this chiral column ($\alpha = 1.11$ (**2**), 1.15 (**10**)). Thus, the acidic amidic hydrogen of the CDCPC strongly contributes to determine the affinity of the analyte toward the selector participating in the C≡N···H-N HB, but less to enantioselectivity.

Among all compounds, 1,3-disubstituted **7** and **8** showed an interesting behaviour with very high affinity for the amylose-based selectors by using methanol-containing MPs (Tables S9 and S10). The same behaviour was not observed for the 1,2-analogues **4** and **5**.

*3.4 Enantioseparation of compounds **7** and **8**: CDMPC vs ADMPC*

As shown in Figure 4, 1,3-disubstituted ferrocenes **7** and **8** showed a complementary behaviour on C-1 as the MP changes, and in both cases two mechanisms seem to control enantioseparation on this column depending on MP polarity:

i) a mechanism based on polar interactions occurring with mixture A, which proved to be more effective, in terms of selectivity, for compound **8** (R = naphthyl) ($\alpha = 1.25$) compared to derivative **7** (R = Ph) ($\alpha = 1.08$). The addition of methanol to mixture A, or the use of pure MeOH as a MP, appeared to be detrimental for the enantioseparation in both cases;

ii) a mechanism occurring under hydrophobic conditions when increasing amounts of water (5% and 10%) were added to the MP consisting of pure methanol. In these cases, the separation system behaves as a typical reversed-phase system, and selectivity factors increased with increasing amount of water additive [52]. Under these conditions, compound **7** ($\alpha = 1.19$) was enantioseparated better than compound **8** ($\alpha = 1.09$).

Interestingly, for compound **7** the transition between the two mechanisms is associated with a MP-dependent reversal of EEO, which is *R-S* with A and B as MPs, and *S-R* with pure methanol and aqueous mixtures D and E. Otherwise, the naphthyl derivative **8** retained the same *R-S* elution sequence with all MPs (A-E).

The features of the enantioseparations of compounds **7** and **8** on A-1 were shown to be completely different (Figure 4). In these cases, with mixture A the phenyl derivative **7** was enantioseparated better ($\alpha = 2.27$) than compound **8** ($\alpha = 1.29$), showing an opposite trend compared to the enantioseparations on CDMPC, also in terms of EEO (CDMPC: *R*-*S*; ADMPC: *S*-*R*). On the amylose-based selector, the use of methanol-containing MPs such as B and C increased retention and selectivity producing large enantioseparation for both compounds **7** ($\alpha_B = 8.87$; $\alpha_C = 11.41$) and **8** ($\alpha_B = 4.50$; $\alpha_C = 8.92$). In particular, for compound **7,** the addition of only 2.5% MeOH to the binary mixture A caused the increase of the retention time of the second eluted (*R*)-enantiomer from 11.43 min to 83.46 min, and a further increase to 96.25 min by using pure MeOH as MP. The effect occurred in less degree for compound **8**, the retention time of the second eluted enantiomer changing from 14.08 min to 24.38 and 46.6 min with A, B, and C as MPs, respectively.

The application of van't Hoff analysis allowed for identifying different thermodynamic profiles for compound **7** and **8** as the cause of the different selectivity observed by changing the ADMPC to CDMPC. Thus, retention and selectivity of compounds **7** and **8** on C-1 and A-1 with hex/IPA 95:5 v/v as a MP, were determined at different temperatures from 5 to 45 °C in 5 °C increments (Supplementary material, Table S13). The thermodynamic quantities derived from van't Hoff plots (Figure S7) are reported in Table S14 (Supplementary material). The enantioseparations of both analytes on C-1 were shown to be enthalpy-driven with T_{iso} = 147°C and 85°C for **7** and **8**, respectively. Otherwise, the enantioseparation of **8** on A-1 is entropy-driven ($|T\Delta\Delta S°| > |\Delta\Delta H°|$) and a T_{iso} = -37°C was calculated in this case. An enthalpy-driven process also occurred ($|T\Delta\Delta S°| < |\Delta\Delta H°|$) for the enantioseparation of 7 on A-1, where the difference between the free energies associated to the transfer of the enantiomers from the MP to the selector surfaces is essentially due to a negative enthalpy contribution (-281.3 cal/mol), whereas the entropy term is positive and close to zero (0.78 cal·K-1·mol-1). Indeed, the enantioselectivity is almost independent of the temperature variation. Moving from C-1 to A-1, an increase of the entropy contribution to enantioselection could be determined by comparing the values of

285 the thermodynamic ratio $Q = \Delta\Delta H°/(298\times\Delta\Delta S°)$: **7**, 1.41 (C-1) → 1.21 (A-1); **8**, 1.20 (C-1) → 0.79 (A-
286 1).

287 Large separations for compounds **7** and **8** were also observed on iA-1 (Supporting Information,
288 Figures S8 and S9) and iA-3 (Figures S10 and S11), but not with cellulose-based selectors, showing that
289 the high affinity of the second eluted enantiomers of these compounds toward the selectors is mainly
290 determined by the features of backbone with methanol-containing MP, thus occurring under
291 hydrophobic conditions. With the aim to confirm this feature, we explored the impact of adding polar
292 and nonpolar components to the MP on the retention of the second (*R*)-enantiomer of compounds **7** and
293 **8** by using iA-1 (Figures S8 and S9). Considering that solvents favour and disfavour hydrophobic and
294 polar interactions, respectively, following the order acetonitrile (ACN) < IPA < MeOH < water,
295 changing the aqueous mixture D to MeOH/IPA and MeOH/acetonitrile (ACN) as MPs caused a decrease
296 in the retention of the (*R*)-enantiomer of **7** decreased from 113.10 min to 23.28 and 18.38 min,
297 respectively. Otherwise, by adding 5% water to pure ACN, retention time of the (*R*)-enantiomer
298 increased from 15.12 min to 26.89 min. On this basis, by changing MeOH to ACN in mixture D a drop
299 of retention time of the (*R*)-enantiomer from 113.10 min to 26.89 was observed. On the other hand, the
300 retention factors of the first eluted (*S*)-enantiomer ($0.56 \leq k_2 \leq 3.50$) showed to be less influenced by the
301 polarity of the MP compared to the (*R*)-enantiomer ($2.56 \leq k_2 \leq 27.79$). A similar trend was obtained for
302 compound **8**. The evaluation of the 'dance' of the second peak on the time scale under multimodal
303 conditions, allowed to confirm that the high affinity of the analyte toward amylose-based selectors
304 actually originates from hydrophobic conditions.

305 With the aim to explore the mechanism at the molecular level, a MD simulation was performed by
306 using the (*R*)-enantiomer of compound **7** as selectand, an ADMPC nonamer as selector, and MeOH as a
307 virtual solvent (Fig. 5). The modelling of the experimental enantioseparation confirmed that the (*R*)-
308 enantiomer of compound **7** penetrates deeply in the groove of the selector (Fig. 5a). The selectand
309 remained blocked during 100 ns of MD and confined in a hydrophobic cavity which appeared to be

profiled by six aromatic rings of the selector (Fig. 5b). Interestingly, a HB between the π-ethynyl cloud and the amidic hydrogen of the selector (d = 2.347 Å) was observed to contribute to the binding of the (*R*)-enantiomer into the polymer groove, confirming the pivotal role of this structural element on enantioseparation.

4. CONCLUSION

In this study, the enantioseparation of ferrocenes **1**-**10** has been explored systematically and, as a result, methods for baseline enantioseparations were successfully developed for nine compounds with selectivity factors ranging from 1.20 to 2.92. Otherwise, 1-bromo-2-iodo-ferrocene (**9**) could be only partially enantioseparated, confirming that the enantioseparation of small nonpolar planar chiral ferrocenes remains rather challenging. In most cases, amylose-based CSPs provided better enantioseparation performances compared to cellulose-based ones. Due to the hydrophobic feature of the ferrocenes used in this study as analytes, aqueous methanol-containing MPs allowed for improving enantioseparation performances in several cases.

The impact of π-extended clouds on the enantioseparations was clearly demonstrated, compounds **7** and **8** providing interesting trends and behaviours as both selector and MP features changes. Interestingly, the addition of small (2.5%) percentages of methanol to the Hex/IPA 95:5 increased significantly the affinity of the second eluted enantiomers of compounds **7** and **8**, producing large enantioseparations on amylose-based selectors ranging from 4.69 to 11.41, and from 4.50 to 8.92, respectively.

MD simulations disclosed *a)* the confinement of the analyte in a hydrophobic cavity deeply inside the ADMPC groove and *b)* the stabilization of the selector-selectand complex exerted by a HB between the ethynyl π-cloud and the amidic hydrogen of the selector, as the molecular basis underlying the high affinity of analytes **7** and **8** toward amylose-based selectors.

REFERENCES

[1] Fabbrizzi L. The ferrocenium/ferrocene couple: a versatile redox switch. *Chem Texts.* 2011;6:22. DOI: 10.1007/s40828-020-00119-6

[2] Wilkinson G, Rosenblum M, Whiting MC, Woodward RB. The structure of iron bis-cyclopentadienyl. *J Am Chem Soc*. 1952;74:2125–2126. DOI: 10.1021/ja01128a527

[3] Lotz M, Ireland T, Tappe K, Knochel P. Preparation of new chiral borane-protected P,N-ferrocenyl ligands via a methoxy directed ortho-lithiation. *Chirality* 2000;12:389–395. DOI: 10.1002/(SICI)1520-636X(2000)12:5/6<389::AID-CHIR16>3.0.CO;2-S

[4] Astruc D. Why is ferrocene so exceptional? *Eur J Inorg Chem*. 2017;6–29. DOI: 10.1002/ejic.201600983

[5] Tazi M, Hedidi M, Erb W, Halauko YS, Ivashkevich OA, Matulis VE, Roisnel T, Dorcet V, Bentabed-Ababsa G, Mongin F. Fluoro- and chloroferrocene: from 2- to 3-substituted derivatives. *Organometallics*. 2018;37:2207−2221. DOI: 10.1021/acs.organomet.8b00384

[6] Mamane V, Peluso P, Aubert E, Weiss R, Wenger E, Cossu S, Pale P. Disubstituted ferrocenyl iodo- and chalcogenoalkynes as chiral halogen and chalcogen bond donors. *Organometallics* 2020;39:3936−3950. DOI: 10.1021/acs.organomet.0c00633

[7] Ravutsov M, Dobrikov GM, Dangalov M, Nikolova R, Dimitrov V, Mazzeo G, Longhi G, Abbate S, Paoloni L, Fusè M, Barone V. 1,2-Disubstituted planar chiral ferrocene derivatives from sulfonamide-directed ortho-lithiation: synthesis, absolute configuration, and chiroptical properties. *Organometallics*. 2021;40;578−590. DOI: 10.1021/acs.organomet.0c00712

[8] Dai LX, Tu T, You SL, Deng WP, Hou XL. Asymmetric catalysis with chiral ferrocene ligands. *Acc Chem Res*. 2003;36:659–667. DOI: 10.1021/ar020153m

[9] Cunningham L, Benson A, Guiry PJ. Recent developments in the synthesis and applications of chiral ferrocene ligands and organocatalysts in asymmetric catalysis. *Org Biomol Chem*. 2020;18:9329–9370. DOI: 10.1039/d0ob01933j

[10] Aubert E, Doudouh A, Wenger E, Sechi B, Peluso P, Pale P, Mamane V. Chiral ferrocenyl–iodotriazoles and –iodotriazoliums as halogen bond donors. Synthesis, solid state analysis and catalytic properties. *Eur J Inorg Chem*. **2021**, *submitted*.

[11] Patra M, Gasser G, The medicinal chemistry of ferrocene and its derivatives. *Nat Rev Chem*. 2017;1:0066. DOI: 10.1038/s41570-017-0066

[12] Chuard T, Deschenaux R. Functional liquid-crystalline materials based on ferrocene. *Chimia* 2003;57:597–600. DOI: 10.2533/000942903777678803

[13] Vollmann M, Butenschön H. Synthesis of a functionalized dialkynylferrocene for molecular electronics. *C R Chimie* 2005;8:1282–1285. DOI: 10.1016/j.crci.2005.02.019

[14] Benecke J, Grape ES, Fuß A, Wöhlbrandt S, Engesser TA, Inge AK, Stock N, Reinsch H. Polymorphous indium metal−organic frameworks based on a ferrocene linker: redox activity, porosity, and structural diversity. *Inorg Chem*. 2020;59:9969−9978. DOI: 10.1021/acs.inorgchem.0c01124

[15] Peng L, Feng A, Huo M, Yuan J. Ferrocene-based supramolecular structures and their applications in electrochemical responsive systems. *Chem Commun*. 2014;50:13005−13014. DOI 10.1039/c4cc05192k

[16] Lim JYC, Beer PD. A halogen bonding 1,3-disubstituted ferrocene receptor for recognition and redox sensing of azide. *Eur J Inorg Chem*. 2017;220–224. DOI: 10.1002/ejic.201600805

[17] Ding F, Chen S, Wang H. Computational study of ferrocene-based molecular frameworks with 2,5-diethynylpyridine as a chemical bridge. *Materials*. 2010;3:2668-2683. DOI: 10.3390/ma3042668

[18] Schmiel SF, Butenschön H. New π-extended 1,1'-disubstituted ferrocenes with thioate and dithioate end groups. *Eur J Org Chem* 2021;2388–2401. DOI: 10.1002/ejoc.202100335

[19] Bennett TLR, Wilkinson LA, Lok JMA, O'Toole RCP, Long NJ. Synthesis, electrochemistry, and optical properties of highly conjugated alkynyl-ferrocenes and -biferrocenes. *Organometallics*. 2021;40:1156−1162. DOI: 10.1021/acs.organomet.1c00098

[20] Getty SA, Engtrakul C, Wang L, Liu R, Ke SH, Baranger HU, Yang W, Fuhrer MS, Sita LR. Near-perfect conduction through a ferrocene-based molecular wire. *Phys Rev B*. 2005;71:241401. DOI: 10.1103/PhysRevB.71.241401

[21] Urbano A, del Hoyo AM, Martínez-Carrión A, Carreño MC. Asymmetric synthesis and chiroptical properties of enantiopure helical ferrocenes. *Org Lett*. 2019;21:4623−4627. DOI: 10.1021/acs.orglett.9b01522

[22] Dumele O, Wu D, Trapp N, Goroff N, Diederich F. Halogen bonding of (iodoethynyl)benzene derivatives in solution. *Org Lett.* 2014;16:4722–4725. DOI: 10.1021/ol502099j

[23] Aakeröy CB, Wijethunga TK, Desper J, Đakovic M. Crystal engineering with iodoethynylnitrobenzenes: a group of highly effective halogen-bond donors. *Cryst Growth Des*. 2015;15:3853−3861. DOI: 10.1021/acs.cgd.5b00478

[24] Peluso P, Mamane V, Aubert E, Dessì A, Dallocchio R, Dore A, Pale P, Cossu S. Insights into halogen bond-driven enantioseparations. *J Chromatogr A*. 2016;1467:228–238. DOI: 10.1016/j.chroma.2016.06.007

[25] Peluso P, Mamane V, Dallocchio R, Dessì A, Villano R, Sanna D, Aubert E, Pale P, Cossu S. Polysaccharide-based chiral stationary phases as halogen bond acceptors: A novel strategy for detection of stereoselective σ-hole bonds in solution. *J Sep Sci*. 2018;41:1247–1256. DOI: 10.1002/jssc.201701206

[26] Peluso P, Gatti C, Dessì A, Dallocchio R, Weiss R, Aubert E, Pale P, Cossu S, Mamane V. Enantioseparation of fluorinated 3-arylthio-4,4'-bipyridines: Insights into chalcogen and π-hole bonds in high-performance liquid chromatography. *J Chromatogr A* 2018;1567:119–129. DOI: 10.1016/j.chroma.2018.06.060

[27] Peluso P, Dessì A, Dallocchio R, Sechi B, Gatti C, Chankvetadze B, Mamane V, Weiss R, Pale P, Aubert E, Cossu S. Enantioseparation of 5,5'-dibromo-2,2'-dichloro-3-selanyl-4,4'-bipyridines on polysaccharide-based chiral stationary phases: exploring chalcogen bonds in liquid-phase chromatography. *Molecules*. 2021;26:221. DOI: 10.3390/molecules26010221

[28] Yamazaki Y, Morohashi N, Hosono K. High-performance liquid chromatographic determination of optical purity of planar chiral organometallic compounds resolved by enzymic transformations. *J Chromatogr A*. 1991;542:129−136. DOI: 10.1016/S0021-9673(01)88753-7

[29] Tsukazaki M, Tinkl M, Roglans A, Chapell BJ, Taylor NJ, Snieckus V. Direct and highly enantioselective synthesis of ferrocenes with planar chirality by (-)-sparteine-mediated lithiation. *J Am Chem Soc*. 1996;118:685–686. DOI: /10.1021/ja953246q

[30] Thorat RA, Jain S, Sattar M, Yadav P, Mandhar Y, Kumar S. Synthesis of chiral-substituted 2-aryl-ferrocenes by the Catellani reaction. *J Org Chem*. 2020;85:14866−14878. DOI: 10.1021/acs.joc.0c01360

[31] Patti A, Pedotti S, Sanfilippo C. Comparative HPLC enantioseparation of ferrocenylalcohols on two cellulose-based chiral stationary phases. *Chirality*. 2007;19:344−351. DOI: 10.1002/chir.20386

[32] Ogasawara M, Enomoto Y, Uryu M, Yang X, Kataoka A, Ohnishi A. Application of polysaccharide-based chiral HPLC columns for separation of nonenantiomeric isomeric mixtures of organometallic compounds. *Organometallics*. 2019;38:512−518. DOI: 10.1021/acs.organomet.8b00819

[33] Okamoto Y, Kawashima M, Hatada K. Useful chiral packing materials for high-performance liquid chromatographic resolution of enantiomers: phenylcarbamates of polysaccharides coated on silica gel. *J Am Chem Soc*. 1984;106:5357−5359. DOI: 10.1021/ja00330a057

[34] Okamoto Y, Kawashima M, Yamamoto K, Hatada K. Useful chiral packing materials for high-performance liquid chromatographic resolution. Cellulose triacetate and tribenzoate coated on microporous silica gel. *Chem Lett*. 1984;13:739−742. DOI: 10.1246/cl.1984.739

[35] Li W, Zhang W, Wang X, Dou J, Chen L, Li Y. Chiral separation of novel chiral tetrahedrone-type clusters on a cellulose tris(3,5-dimethylphenylcarbamate) chiral stationary phase. *Anal Chim Acta*. 2003;495:77–83. DOI: 10.1016/j.aca.2003.08.038

[36] Zhu X, Cai Y, Zhang W, Chen L, Li Y. Enantioseparation of novel chiral heterometal tetrahedral clusters by high-performance liquid chromatography. *J Chromatogr A*. 2003;1002:231–236. DOI: 10.1016 /S0021-9673(03)00655-1

[37] Wang X, Li W, Zhao Q, Li Y, Chen L. Normal-phase HPLC enantioseparation of novel chiral metal tetrahedrane-type clusters on an amylose-based chiral stationary phase. *Anal Sci*. 2005;21:125–128. DOI: 10.2116/analsci.21.125

[38] Gallinella B, Bucciarelli L, Zanitti L, Ferretti R, Cirilli R. Direct separation of the enantiomers of oxaliplatin on a cellulose-based chiral stationary phase in hydrophilic interaction liquid chromatography mode. *J Chromatogr A*. 2014;1339:210–213. DOI: 10.1016/j.chroma.2014.02.071

[39] Citti C, Battisti UM, Ciccarella G, Maiorano V, Gigli G, Abbate S, Mazzeo G, Castiglioni E, Longhi G, Cannazza G. Analytical and preparative enantioseparation and main chiroptical properties of Iridium(III) bis(4,6-difluorophenylpyridinato)picolinato. *J Chromatogr. A*. 2016;1467:335–346. DOI: 10.1016/j.chroma.2016.05.059

[40] Dayaker G, Sreeshailam A, Chevallier F, Roisnel T, Krishna PR, Mongin F. Deprotonative metallation of ferrocenes using mixed lithium−zinc and lithium−cadmium combinations. *Chem Commun.* 2010;46: 2862−2864. DOI: 10.1039/B924939G

[41] Frisch MJ, Trucks GW, Schlegel HB, Scuseria GE, Robb MA, Cheeseman JR, Scalmani G, Barone V, Mennucci B, Petersson GA, Nakatsuji H, Caricato M, Hratchian X, Li HP, Izmaylov

AF, Bloino J, Zheng G, Sonnenberg JL, Hada M, Ehara M, Toyota K, Fukuda R, Hasegawa J, Ishida M, Nakajima T, Honda Y, Kitao O, Nakai H, Vreven T, Montgomery Jr. JA, Peralta JE, Ogliaro F, Bearpark M, Heyd JJ, Brothers E, Kudin KN, Staroverov VN, Keith T, Kobayashi R, Normand J, Raghavachari K, Rendell A, Burant JC, Iyengar SS, Tomasi J, Cossi M, Rega N, Millam JM, Klene M, Knox JE, Cross JB, Bakken V, Adamo C, Jaramillo J, Gomperts R, Stratmann RE, Yazyev O, Austin AJ, Cammi R, Pomelli C, Ochterski JW, Martin RL, Morokuma K, Zakrzewski VG, Voth G, Salvador P, Dannenberg JJ, Dapprich S, Daniels AD, Farkas O, Foresman JB, Ortiz J, Cioslowski J, Fox DJ. Gaussian 09, Revision B. 01, Inc.Gaussian, C.T. Wallingford, 2010.

[42] Lu T, Chen F. Multiwfn: A multifunctional wavefunction analyser. *J Comp Chem*. 2012;33:580–592. DOI: 10.1002/jcc.22885

[43] Lu T, Chen F. Quantitative analysis of molecular surface based on improved Marching Tetrahedra algorithm. *J Mol Graph Model*. 2012;38:314–323. DOI: 10.1016/j.jmgm.2012.07.004

[44] Chankvetadze B. Recent trends in preparation, investigation and application of polysaccharide-based chiral stationary phases for separation of enantiomers in high-performance liquid chromatography. *Trends Anal Chem.* 2020;122:115709. DOI: 10.1016/j.trac.2019.115709

[45] Peluso P, Sechi B, Lai G, Dessì A, Dallocchio R, Cossu S, Aubert E, Weiss R, Pale P, Mamane V, Chankvetadze B. Comparative enantioseparation of chiral 4,4’-bipyridine derivatives on coated and immobilized amylose-based chiral stationary phases. *J Chromatogr A*. 2020;1625:461303. DOI: 10.1016/j.chroma.2020.461303

[46] Chankvetadze B, Yamamoto C, Okamoto Y. Enantioseparation of selected chiral sulfoxides using polysaccharide-type chiral stationary phases and polar organic, polar aqueous–organic and normal-phase eluents. *J Chromatogr A*. 2001;922:127–137. DOI: 10.1016/S0021-9673(01)00958-X

[47] Chankvetadze B. Recent developments on polysaccharide-based chiral stationary phases for liquid-phase separation of enantiomers. *J Chromatogr A.* 2012;1269:26–51. DOI: 10.1016/j.chroma.2012.10.033

[48] Zhao B, Oroskar PA, Wang X, House D, Oroskar A, Oroskar A, Jameson CJ, Murad S. The composition of the mobile phase affects the dynamic chiral recognition of drug molecules by the chiral stationary phase. *Langmuir*. 2017;33:11246–11256. DOI: 10.1021/acs.langmuir.7b02337

[49] Horváth S, Németh G. Hysteresis of retention and enantioselectivity on amylose tris(3,5-dimethylphenylcarbamate) chiral stationary phases in mixtures of 2-propanol and methanol. *J Chromatogr A*. 2018;1568:149–159. DOI: 10.1016/j.chroma.2018.07.033

[50] Chankvetadze B. Polysacchride-based chiral stationary phases for enantioseparations by high-performance liquid chromatography: an overview, in Scriba GKE, (Ed) Chiral separations: methods and protocols, Methods in molecular biology; vol 1985, Springer Science + Business Media, LLC, part of Springer Nature, 2019; pp 93–126.

[51] Shedania Z, Kakava R, Volonterio A, Farkas T, Chankvetadze B. Separation of enantiomers of chiral sulfoxides in high-performance liquid chromatography with cellulose-based chiral selectors using methanol and methanol-water mixtures as mobile phases. *J Chromatogr A.* 2018;1557:62–74. DOI: 10.1016/j.chroma.2018.05.002

[52] Chankvetadze B, Yamamoto C, Okamoto Y, Enantioseparation of selected chiral sulfoxides using polysaccharide-type chiral stationary phases and polar organic, polar aqueous–organic and normal-phase eluents. *J Chromatogr A.* 2001;922:127–137. DOI: 10.1016/S0021-9673(01)00958-X

FIGURE CAPTIONS

FIGURE 1 Structures and numbering of chiral ferrocenes **1-10**

FIGURE 2 The highest occupied molecular orbitals (HOMO) (contour value = 0.02 au) for compounds **3-5** (a-c), and electrostatic potential isosurface (V_S) (isovalue 0.002 au) of compound **6** (d) (DFT/B3LYP/def2TZVPP; color legend: minimum and maximum V_S values are depicted in red and blue, respectively, and colors in between (orange, yellow, green) depict intermediate values)

FIGURE 3 Rate of baseline enantioseparations of compounds **1-8** and **10** under multimodal elution conditions

FIGURE 4 Comparison of the enantioseparation traces of compounds **7** and **8** on C-1 and A-1 under multimodal elution conditions

FIGURE 5 Representative snapshot from the simulated MD trajectories (100 ns) of (*R*)-**7** complex with ADMPC (solvent box, MeOH): a) electron density surface (legend colours: green, aromatic ring; red, C=O; blue, N-H; grey, Ph + Cp + C≡C of (*R*)-**7**; magenta, iodine), b) tube model of the (*R*)-**7**/ADMPC complex (legend colours: orange, Ph + Cp + Fe + C≡C of (*R*)-**7**; magenta, iodine; green, aromatic rings featuring and delimiting the hydrophobic binding cavity of ADMPC)

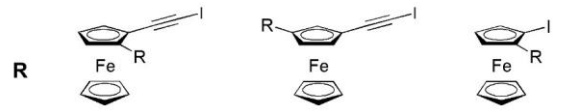

Br	**1**	**6**	**9**
CN	**2**		**10**
Me	**3**		
Ph	**4**	**7**	
2-Naph	**5**	**8**	

516

517 **FIGURE 1** Structures and numbering of chiral ferrocenes **1-10**

518

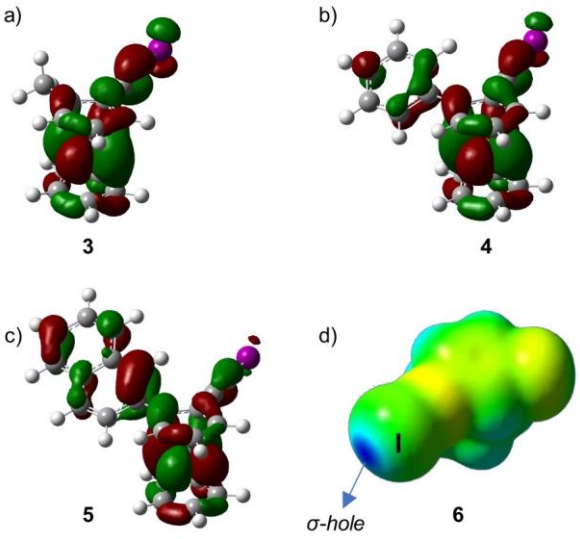

519

520 **FIGURE 2** The highest occupied molecular orbitals (HOMO) (contour value = 0.02 au) for compounds **3-5** (a-c), and
521 electrostatic potential isosurface (V_S) (isovalue 0.002 au) of compound **6** (d) (DFT/B3LYP/def2TZVPP; color legend:
522 minimum and maximum V_S values are depicted in red and blue, respectively, and colors in between (orange, yellow, green)
523 depict intermediate values)

524

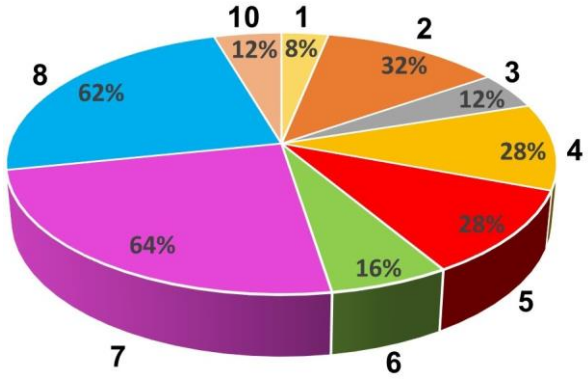

FIGURE 3 Rate of baseline enantioseparations of compounds **1**-**8** and **10** under multimodal elution conditions

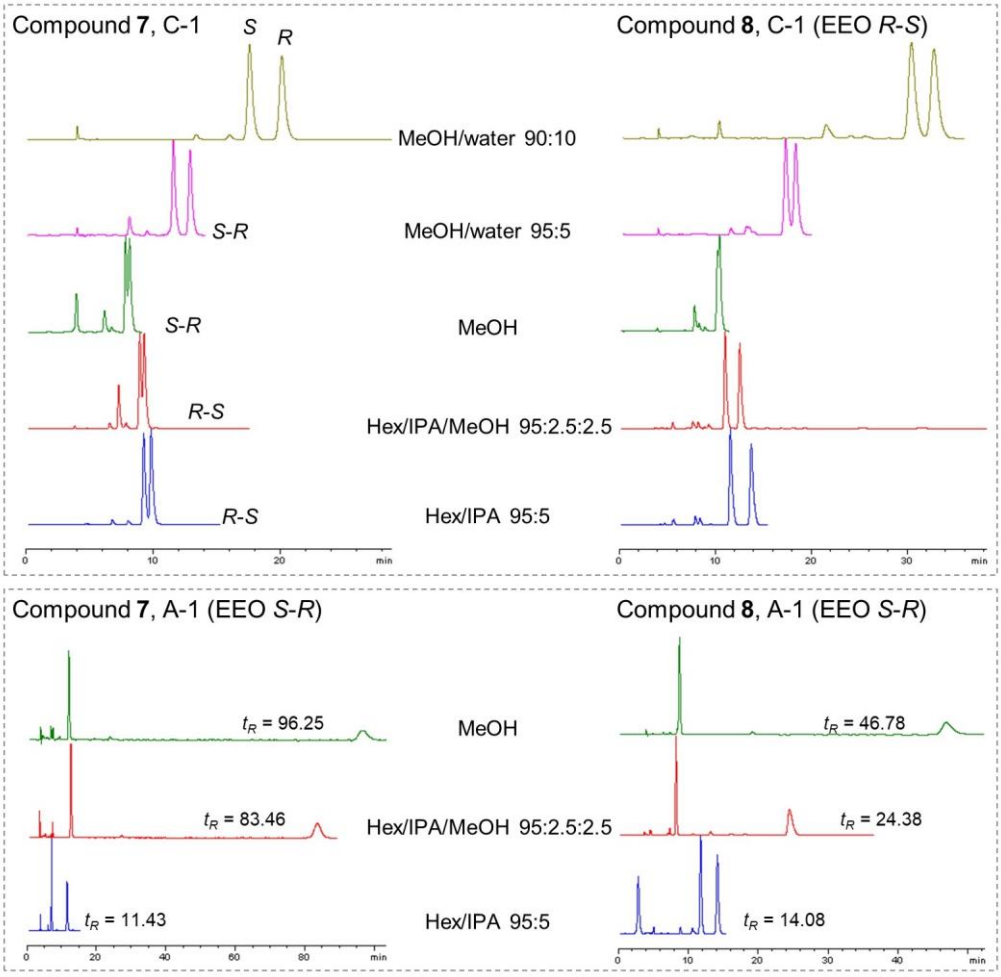

FIGURE 4 Comparison of the enantioseparation traces of compounds **7** and **8** on C-1 and A-1 under multimodal elution conditions

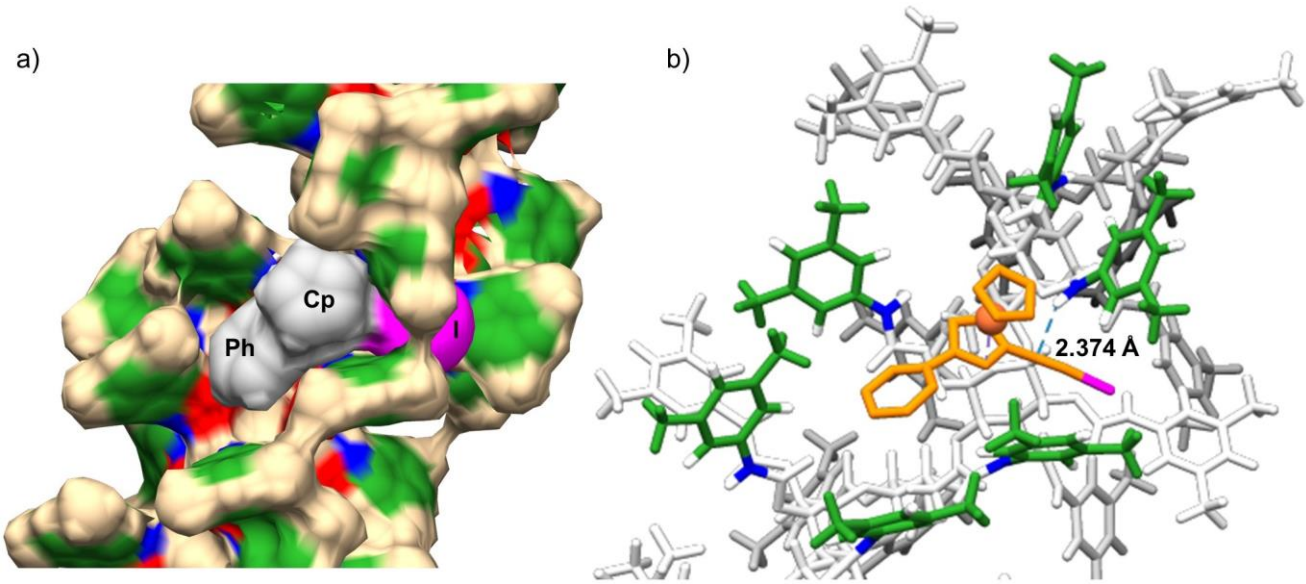

FIGURE 5 Representative snapshot from the simulated MD trajectories (100 ns) of (*R*)-**7** complex with ADMPC (solvent box, MeOH): a) electron density surface (legend colours: green, aromatic ring; red, C=O; blue, N-H; grey, Ph + Cp + C≡C of (*R*)-**7**; magenta, iodine), b) tube model of the (*R*)-**7**/ADMPC complex (legend colours: orange, Ph + Cp + Fe + C≡C of (*R*)-**7**; magenta, iodine; green, aromatic rings featuring and delimiting the hydrophobic binding cavity of ADMPC)

TABLE 1 $V_{S,max}$ and $V_{S,min}$ values (a.u.) associated with the main recognition sites (carbamate N–H, C=O, and Ar) of cellulose- and amylose-based selectors used in the study (DFT/B3LYP/def2TZVPP)

Chiral selector	Side chain	$V_{S,max}$ (N–H)	$V_{S,min}$ (C=O)	$V_{S,min}$ (Ar)
CDMPC/ADMPC	3,5-dimethylphenylcarbamate	0.0843	-0.0625	-0.0271
CDCPC	3,5-dichlorophenylcarbamate	0.0990	-0.0536	-0.0066
ACMPC	3-chloro-5-methylphenylcarbamate	0.0914	-0.0595	-0.0163

TABLE 2 Chromatographic parameters (t, k, α) for optimized baseline enantioseparations of *rac*-**1**-**8** and **10** on polysaccharide carbamate-based chiral columns under multimodal elution conditions

Compound	Column	MP	t_1 [min]	t_2 [min]	k_1	k_2	α	EEO
1	A-1	E	7.42	8.11	0.88	1.05	1.20	*S-R*
2	A-1	D	4.80	5.80	0.23	0.49	2.13	*S-R*
3	iA-3	E	6.79	8.09	0.71	1.03	1.46	*S-R*
4	iA-3	C	4.79	5.63	0.22	0.44	1.97	*R-S*
5	iC-5	A	7.22	9.29	0.95	1.51	1.59	*S-R*
6	A-1	C	7.91	8.68	1.05	1.25	1.19	*R-S*
7	iA-3	A	6.16	11.03	0.70	2.05	2.92	*S-R*
8	iA-3	A	7.34	10.12	1.03	1.80	1.75	*S-R*
10	C-1	D	6.18	7.60	0.55	0.90	1.65	*Y-X*

Abbreviation: EEO, enantiomer elution order; the notation *X* or *Y* is reported for unknown absolute configuration; C-1, Lux Cellulose 1; iC-5, Lux i-Cellulose-5; A-1, Lux Amylose-1; iA-1, Lux i-Amylose-1; iA-3, Lux i-Amylose-3; A, Hex/IPA 95:5 v/v; B, Hex/IPA/MeOH 95:2.5:2.5 v/v/v; C, MeOH 100%; D, MeOH/water 95:5 v/v; E, MeOH:water 90:10 v/v